April 2001 • NREL/SR-500-29492

Subcontractor Report

WindPACT Turbine Design Scaling Studies Technical Area 1–Composite Blades for 80- to 120-Meter Rotor

March 21, 2000 – March 15, 2001

Dayton A. Griffin
Global Energy Concepts
Kirkland, Washington

National Renewable Energy Laboratory

1617 Cole Boulevard
Golden, Colorado 80401-3393

NREL is a U.S. Department of Energy Laboratory
Operated by Midwest Research Institute • Battelle • Bechtel

Contract No. DE-AC36-99-GO10337

April 2001 • NREL/SR-500-29492

WindPACT Turbine Design Scaling Studies Technical Area 1–Composite Blades for 80- to 120-Meter Rotor

March 21, 2000 – March 15, 2001

Dayton A. Griffin
Global Energy Concepts
Kirkland, Washington

NREL Technical Monitor: Alan Laxson

Prepared under Subcontract No. YAM-0-30203-01

National Renewable Energy Laboratory

1617 Cole Boulevard
Golden, Colorado 80401-3393

NREL is a U.S. Department of Energy Laboratory
Operated by Midwest Research Institute • Battelle • Bechtel

Contract No. DE-AC36-99-GO10337

NOTICE

Available electronically at http://www.doe.gov/bridge

Available for a processing fee to U.S. Department of Energy
and its contractors, in paper, from:

U.S. Department of Energy
Office of Scientific and Technical Information
P.O. Box 62
Oak Ridge, TN 37831-0062
phone: 865.576.8401
fax: 865.576.5728
email: reports@adonis.osti.gov

Available for sale to the public, in paper, from:

U.S. Department of Commerce
National Technical Information Service
5285 Port Royal Road
Springfield, VA 22161
phone: 800.553.6847
fax: 703.605.6900
email: orders@ntis.fedworld.gov
online ordering: http://www.ntis.gov/ordering.htm

Printed on paper containing at least 50% wastepaper, including 20% postconsumer waste

Executive Summary

The United States Department of Energy (DOE) through the National Renewable Energy Laboratory (NREL) implemented the Wind Partnership for Advanced Component Technologies (WindPACT) program. As part of the WindPACT program, Global Energy Concepts, LLC (GEC), was awarded contract number YAM-0-30203-01 to examine Technical Area 1—Blade Scaling, Technical Area 2—Turbine Rotor and Blade Logistics, and Technical Area 3—Self-Erecting Towers. This report documents the results of GEC's Technical Area 1—Blade Scaling. The primary objectives of the Blade-Scaling Study are to assess the scaling of current materials and manufacturing technologies for blades of 40 to 60 meters in length, and to develop scaling curves of estimated cost and mass for rotor blades in that size range.

Approach

We investigated the scaling of current materials and manufacturing technologies for wind turbine blades of 40 to 60 meters in length. Direct design calculations were used to construct a computational blade-scaling model, which was then used to calculate structural properties for a wide range of aerodynamic designs and rotor sizes. Industry manufacturing experience was used to develop cost estimates based on blade mass, surface area, and the duration of the assumed production run.

The structural design model was also used to perform a series of parametric analyses. The results quantify the mass and cost savings possible for specific modifications to the baseline blade design, demonstrate the aerodynamic and structural trade-offs involved, and identify the constraints and practical limits to each modification.

Conclusions and Results

The scaling-model results were compared with mass data for current commercial blades. For a given blade design, the scaling model indicates that blade mass and costs scale as a near-cubic of rotor diameter. In contrast, commercial blade designs have maintained a scaling exponent closer to 2.4 for lengths ranging between 20 and 40 meters. Results from the scaling study indicate that:

- To realize this lower scaling exponent on cost and mass has required significant evolution of the aerodynamic and structural designs.
- Commercial blades at the upper end of the current size range are already pushing the limits of what can be achieved using conventional manufacturing methods and materials.
- For even larger blades, avoiding a near-cubic mass increase will require basic changes in:
  - Materials, such as carbon or glass/carbon hybrids.
  - Manufacturing processes that can yield better mean properties and/or reduced property scatter through improvements in fiber alignment, compaction, and void reduction. The extent to which such improvements would result in lower blade masses may be constrained by blade stiffness requirements.
  - Load-mitigating rotor designs.

For the scaling results presented in this report, the basic material and manufacturing process remained unchanged. As such, a reduction in mass will correspond to a reduction of production

blade costs in the same proportion. However, this will not hold true for mass savings realized through changes in materials, process, and rotor design. In evaluating each such change, the implications on both mass and cost must be considered.

As part of the cost analysis, it was shown that the "learning curve" required to achieve a mature production process has a meaningful effect on blade costs for the range of rotor sizes considered. A production rate of 200 megawatts (MW) per year implies 800 blades at 750 kilowatts (kW), but only 120 blades at 5 MW. Therefore, the cost penalty for initial production cycles has an increasing impact on the first-year production costs as rotor sizes increase, and a complete cost assessment depends on both annual production rates and the extent (number of years) of sustained production.

The results of the scaling analysis are shown in the table below.

Blade Mass and Cost for Rotors between 750 kW and 5 MW (5-year production)

Radius	Rating	Area*	Mass (kg)		Average Cost per Blade			Rotor Costs	
(m)	(kW)	(m^2)	Blade	Root	Fixed	Prod.	Total	$/kW	$/MWh/yr
23.3	750	66.3	1577	111	$115	$19,100	$19,215	$76.9	$25.1
32.9	1500	132.6	4292	243	$520	$51,850	$52,370	$104.7	$31.4
38.0	2000	176.8	6528	336	$970	$79,230	$80,200	$120.3	$34.9
40.8	2300	203.3	8010	388	$1,320	$97,495	$98,815	$128.9	$36.6
46.6	3000	265.2	11,783	515	$2,350	$144,910	$147,260	$147.3	$40.8
53.8	4000	353.6	17,961	681	$4,405	$224,395	$228,800	$171.6	$46.0
60.2	5000	442.0	24,869	851	$7,180	$316,590	$323,770	$194.3	$50.8

* Blade surface area

To assist with the interpretation of this table, scaling exponents as a function of rotor diameter have been developed for several key parameters. The results are presented in the following table.

Scaling Exponents: 2.3 kW to 5 MW

Parameter	Scaling Exponent
Energy production	2.22
Blade mass	2.87
Blade costs	3.03
Rotor cost per kW capacity ($/kW)	1.04
Rotor cost per energy capture ($/MWh/yr)	0.82

Because of the assumed increase in hub height with rotor size and associated wind shear, the energy capture scales more rapidly than the rotor swept area (exponent of 2.22). Because the scaling was performed for a fixed-blade design, the mass exponent is slightly less than cubic. However, due to the impact of the learning-curve costs on the five-year production scenario, the blade cost exponent is slightly greater than cubic. The blade cost per installed kilowatt is shown to increase in a near-linear fashion with diameter, and the cost per energy capture scales as the diameter to an exponent of 0.82.

The cost estimates presented above are appropriate for the assumptions and design modeled. It should be noted that the same general trend would result for any fixed-blade design that is scaled over the same range of ratings. To realize lower exponents on blade cost and mass requires evolution of the design and/or manufacturing process as the rotors become larger.

Table of Contents

List of Figures

List of Tables

Nomenclature

AEP	annual energy production
c	chord length (m)
C_{ia}	partial safety factors for laminate materials
c_{max}	maximum blade chord (% R)
C_P	rotor power coefficient
C_{Pmax}	maximum rotor power coefficient
D	rotor diameter (m)
EI_{Edge}	edgewise bending stiffness (N-m^2)
EI_{Flap}	flapwise bending stiffness (N-m^2)
h_{hub}	rotor hub height (m)
kW	kilowatt
m	meters
N	number of loading cycles for fatigue analysis
MW	megawatt
P_{rated}	Rated power output of turbine (kW)
R	rotor radius (m)
R_f	fatigue bending load ratio (minimum/maximum bending moment)
r/R	spanwise blade station (%)
S	blade surface area
t	physical thickness of a blade section (m)
t/c	airfoil thickness-to-chord (%)
TSR	tip-speed ratio
TSR_{Design}	design tip-speed ratio
x/c	distance along airfoil chord
y/c	distance perpendicular to airfoil chord
$V_{cut\text{-}out}$	wind speed at turbine cut-out (m/s)
V_{mean}	annual average wind speed at hub height (m/s)
V_{rated}	wind speed at turbine rated power (m/s)
ε-N	strain-cycle curve for fatigue analysis
η_{DT}	drivetrain efficiency
ρ	air density (kg/m^3)
υ_f	volume fraction of fiber in composite laminate
ϖ_f	weight fraction of fiber in composite laminate

1. Introduction

1.1 Background

The United States Department of Energy (DOE), through the National Renewable Energy Laboratory (NREL) has implemented the Wind Partnership for Advanced Component Technologies (WindPACT) program. This program explores advanced technologies that decrease the cost of energy (COE) from wind turbines. The initial step in the WindPACT program is a series of preliminary scaling studies intended to bound the optimum sizes for future turbines, help define sizing limits for certain critical technologies, and explore the potential for advanced technologies to contribute to reduced COE as turbine scales increase. Four technical areas were identified for examination in this initial phase.

Global Energy Concepts, LLC (GEC), was awarded contract number YAM-0-30203-01 to examine Technical Area 1—Blade Scaling, Technical Area 2—Turbine Rotor and Blade Logistics, and Technical Area 3—Self-Erecting Towers. This report documents the results of GEC's Technical Area 1 study. The primary objectives of the Blade-Scaling Study are to assess the scaling of current materials and manufacturing technologies for blades of 40 to 60 meters (m) in length, and to develop scaling curves of estimated cost and mass for rotor blades in that size range.

To perform this scaling study, a computational modeling tool was developed. The model was then used to calculate structural properties for a wide range of aerodynamic designs and rotor sizes, to quantify possible mass and cost reductions from modifications to the baseline design, and to identify limitations to the economical scaling of the current commercial approach to blade design and manufacture.

1.2 Project Specifications and Design Criteria

1.2.1 Original RFP Specifications

The original NREL Request for Proposals (RFP) included the following specifications for the blade scaling study:

- three blades, upwind rotor with rigid hub and full-span pitch control
- blade flapwise natural frequency between 1.5 and 2.5 per revolution
- blade edgewise natural frequency greater than 1.5 times flapwise natural frequency
- rotor solidity between 2% and 5%
- variable speed operation with maximum power coefficient = 0.50
- maximum tip speed = 85 m/s
- air density = 1.225 kg/m^3
- turbine hub height = 1.3 times rotor diameter
- annual mean wind speed at 10 m height = 5.8 m/s
- Rayleigh distribution of wind speed
- vertical wind shear power exponent = 0.143
- rated wind speed = 1.5 times annual average at hub height
- cut out wind speed = 3.5 times annual average at hub height

These specifications were used to derive relationships between rotor size and rating. From the original WindPACT RFP:

$$V_{mean}(m/s) = 5.8 \cdot \left(\frac{h_{hub}}{10\,\mathrm{m}} \right)^{0.143} \quad \text{(Eqn. 1)}$$

$$V_{rated} = 1.5 \cdot V_{mean} \quad \text{(Eqn. 2)}$$

$$h_{hub} = 1.3 \cdot D \quad \text{(Eqn. 3)}$$

where

V_{mean} ≡ annual average wind speed at hub height (m/s)
V_{rated} ≡ wind speed at turbine rated power (m/s)
h_{hub} ≡ rotor hub height (m)
D ≡ rotor diameter (m).

The turbine system power output at rated wind speed is given by:

$$P_{rated} = \eta_{DT} \cdot C_P \cdot 0.5\rho \cdot (V_{rated})^3 \cdot \pi \cdot \frac{D^2}{4} \quad \text{(Eqn. 4)}$$

where

η_{DT} ≡ drivetrain efficiency
C_P ≡ rotor power coefficient
ρ ≡ air density (kg/m^3).

Assuming η_{DT} = 0.925, C_P = 0.5, and ρ = 1.225 kg/m^3, combining equations 1 through 4, and solving for D yields:

$$D\,(\mathrm{m}) = \left(\frac{P_{rated}}{60.0} \right)^{0.411} \quad \text{(Eqn. 5)}$$

Table 1 provides a summary of the turbine parameters implied by the original WindPACT specifications, for system power ratings ranging from 750 kW to 5 MW.

Table 1. Turbine Parameters as Implied by Original RFP Specifications

System Rating (kW)	V_{mean} (m/s)	V_{rated} (m/s)	$V_{cut\text{-}out}$ (m/s)	Rotor Diameter (m)	Rotor Radius (m)	Specific Rating (kW/m^2)	Tower Height (m)
750	7.54	11.31	26.40	48.3	24.2	0.410	62.8
1500	7.86	11.78	27.50	64.2	32.1	0.464	83.5
3000	8.18	12.27	28.64	85.4	42.7	0.524	111.0
5000	8.43	12.65	29.51	105.3	52.6	0.574	136.9

1.2.2 Deviations from Original RFP Specifications

Prior to conducting the Blade-Scaling Study, the parameters in Table 1 were compared with current commercial turbine designs. As a result, some deviations from the original RFP specifications were made.

Figure 1 shows a scatter plot of turbine specific rating for existing rotor designs in the 40 to 80 m diameter range.[1] The solid line in the figure is a linear regression of the commercial blade data, and the dashed line indicates the specific rating trends implied by the original RFP specifications. The trend shown by the linear regression is one of increasing specific rating with rotor size, but with a lower slope than is implied by the criteria of Equations 1 through 4.

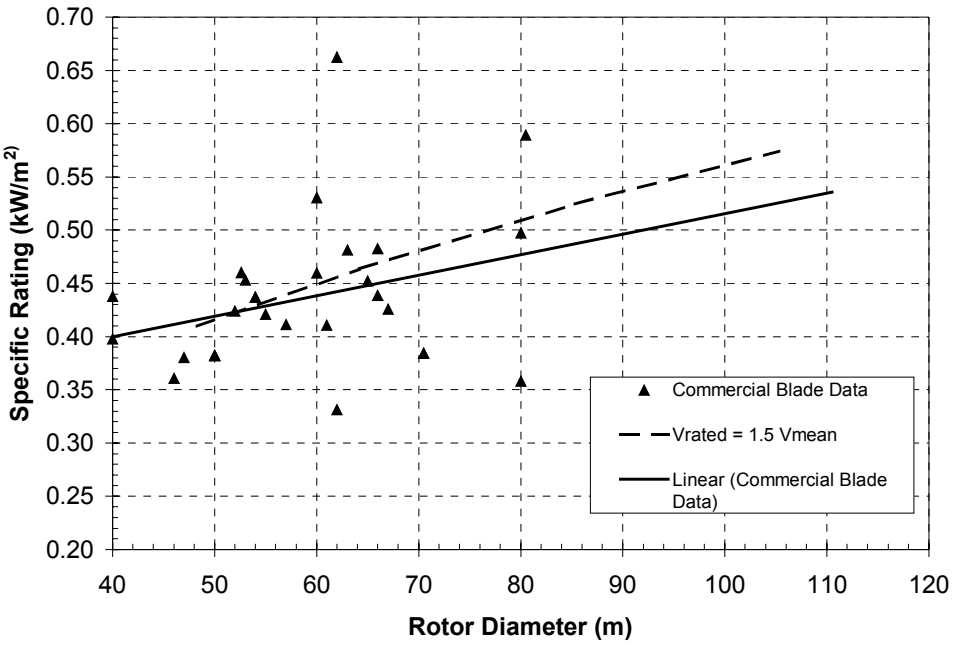

Figure 1. Comparison of specific rating trends

The linear trend line should be interpreted with some caution. The three data points just below 50 m diameter represent rotors of 660-750 kW rating that were "stretched" to as large a size as possible, with the target sites having relatively low wind speeds. Just above 50 m diameter, the data show a step-jump up to rotors of about 1 MW, and although there is some scatter, the specific ratings are all close to 0.44 kW/m^2. At the other end of the size range, current rotors near 80 m diameter show a wide spread in specific rating. The highest specific ratings are targeted for offshore applications, and the lowest specific rating is designed for lower wind speed sites.

Based on this review, GEC concluded that increasing specific rating is not inherently linked to larger rotor sizes, but that the specific rating for each design is determined based on a number of factors, including the target wind regime, terrain, and marketing strategy. As such, the blade-scaling calculations were performed assuming a fixed specific rating fixed of 0.44 kW/m^2. Equations 1 and 3 were applied as given in the original RFP specifications, but the use of a constant specific rating effectively held the rated wind speed as a constant.

Other deviations from the original WindPACT RFP specifications include:

1. The maximum power coefficient (C_{Pmax}) was calculated for each blade design, rather than assumed to be 0.50.
2. During assessment of the turbine power performance:
   a) the maximum tip speed was assumed to be 65 m/s, and
   b) the cut-out wind speed was assumed constant at 22.5 m/s
3. Flapwise natural frequencies in excess of 4.0 per revolution were found to be typical of the blade structural designs developed for this study. A review of available data indicated that these values are representative of existing commercial designs, and as such no attempt was made to constrain blade flapwise natural frequencies to below 2.5 per revolution.

1.2.3 Summary of Design Criteria used for Study

The design criteria and specifications used for this study are summarized in the following bullets, and the resulting turbine sizes and operational parameters are given in Table 2.

- three blades, upwind rotor with rigid hub and full-span pitch control
- blade flapwise natural frequency as calculated, typically greater than 4.0 per revolution
- blade edgewise natural frequency greater than 1.5 times flapwise natural frequency
- rotor solidity between 2% and 5%
- variable speed operation with maximum power coefficient as calculated for each aerodynamic design
- maximum tip speed = 65 m/s (only used in power performance assessment)
- air density = 1.225 kg/m^3
- turbine hub height = 1.3 times rotor diameter
- annual mean wind speed at 10 m height = 5.8 m/s
- Rayleigh distribution of wind speed
- vertical wind shear power exponent = 0.143
- constant specific rating of 0.44 kW/m^2

Table 2. Turbine Parameters used for Scaling Study

System Rating (kW)	V_{mean} (m/s)	V_{rated} (m/s)	$V_{cut\text{-}out}$ (m/s)	Rotor Diameter (m)	Rotor Radius (m)	Specific Rating (kW/m^2)	Tower Height (m)
750	7.50	12.5	22.5	46.6	23.3	0.44	60.6
1500	7.89	12.5	22.5	65.9	32.9	0.44	85.6
3000	8.29	12.5	22.5	93.2	46.6	0.44	121.1
5000	8.59	12.5	22.5	120.4	60.2	0.44	156.4

It should be noted that the tower height, V_{mean}, V_{rated}, and $V_{cut\text{-}out}$ were only used during the assessment of turbine power performance. Blade production costs were estimated assuming a production level of 200 MW rated capacity per year. All structural design calculations were performed assuming a Class 1 50-year extreme wind speed per the International Electrotechnical Commission (IEC) 61400-1 standard.[2]

2. Modeling Approach

2.1 Overview

The scaling model was constructed on the basis of direct aerodynamic and structural-design calculations. A baseline set of design parameters (airfoil shapes, structural arrangement, materials, and manufacturing method) was selected to be consistent with current commercial designs. Using the baseline configuration, a matrix of aerodynamic and structural designs were developed and analyzed. The results were used to construct a model that can be used in an inverse fashion—solving for the required structure when given geometry, loads, and structural-design criteria as input. Industry manufacturing experience was used to develop cost estimates based on blade mass, surface area, and the duration of the assumed production run.

Often, a blade structural model may be based on a greatly simplified sectional representation, so that a closed-form solution is obtained and/or computational complexity is minimized.[3,4] A simplified sectional representation is particularly useful if structural calculations are desired at a large number of blade spanwise stations.

A distinctly different modeling approach was taken. Using a series of detailed structural analyses performed at relatively coarse spacing in the spanwise direction (5, 7, 25, 50, 75 and 100% span), the results of those analyses were used to infer the blade properties at intermediate stations. This approach provided a tool that can be used to parametrically examine the impact of detailed design features changes on blade mass and cost. The following sections describe the elements of the model and how those elements are integrated in the computational modeling tool.

2.2 Aerodynamic Designs

As described in Section 1.2.3, the turbine configuration selected for this study is a three-bladed, upwind rotor with a rigid hub, full-span pitch control, and full variable-speed operation. Aerodynamic performance for each design is indicated by the rotor C_P-TSR curve, maximum rotor power coefficient (C_{Pmax}), and calculated energy production. Rotor dimensions are described in terms of radius, R, and sizing assumes a constant specific power rating of 0.44 kW/m^2. The resulting relationship between the rotor radius and rating was summarized in Table 2.

Figure 2 is a graph of a typical planform, with a linear taper from the maximum chord location (25% r/R) to the blade tip. The circular blade root is located at 5% r/R. The blade shape is assumed to remain circular to 7% r/R, before transitioning to a pure airfoil shape located at 25% r/R.

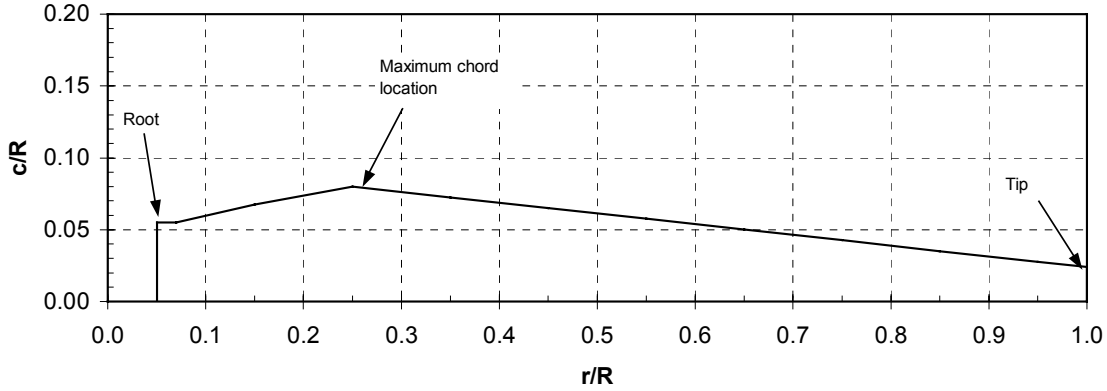

Figure 2. Typical blade planform

Several of the National Renewable Energy Laboratory (NREL) S-series airfoils were considered for use in this study.[5] The S818/S825/S826 family was identified as having desirable aerodynamic properties, but the airfoils were deemed to be too thin for efficient application to large blades (assuming current commercial materials are used). A more structurally suitable set of airfoil shapes was therefore derived by scaling the S818/S825/S826 foils, and by the addition of a finite-thickness trailing edge. The shape modifications, and locations of airfoils along the blade, are summarized in Table 3; the resulting shapes are shown in Figure 3. Aerodynamic properties for the modified shapes were calculated using the Eppler Design and Analysis code.[6]

Table 3. Airfoil Shape Modifications (baseline blade)

Airfoil	R (%)	Orig. t/c (%)	Scaled t/c (%)	Trailing-edge thickness (% c)
S818	25	24	27	1.3
S825	75	17	21	1.0
S826	95	14	16	0.75

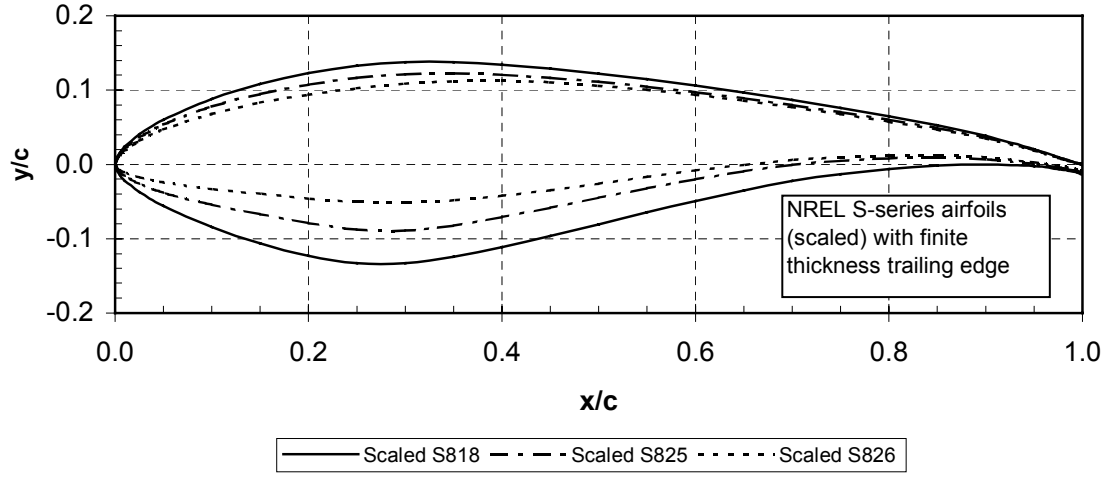

Figure 3. Airfoils used for baseline blade model

The PROPID Design and Analysis code was used to develop aerodynamic designs for a wide range of rotor ratings and planforms.[7] In each case, the PROPID code was used to determine a near-optimal schedule of blade chord and twist. Note that aerodynamic design calculations did not include the optimization of blade stations inboard of 25% r/R. For aerodynamic analysis purposes, the blade was assumed to taper from the 25% r/R section to a circular root located at 5% r/R.

2.3 Baseline Structural Model

A baseline structural arrangement was selected as being representative of current commercial blade designs. The primary structural member is a box-spar, with webs at 15% and 50% chord and a substantial build-up of spar cap material between the webs. The exterior skins and internal shear webs are both sandwich construction with triaxial fiberglass laminate separated by balsa core. This arrangement is depicted in Figure 4, where the thickest airfoil section (25% span station) is shown.

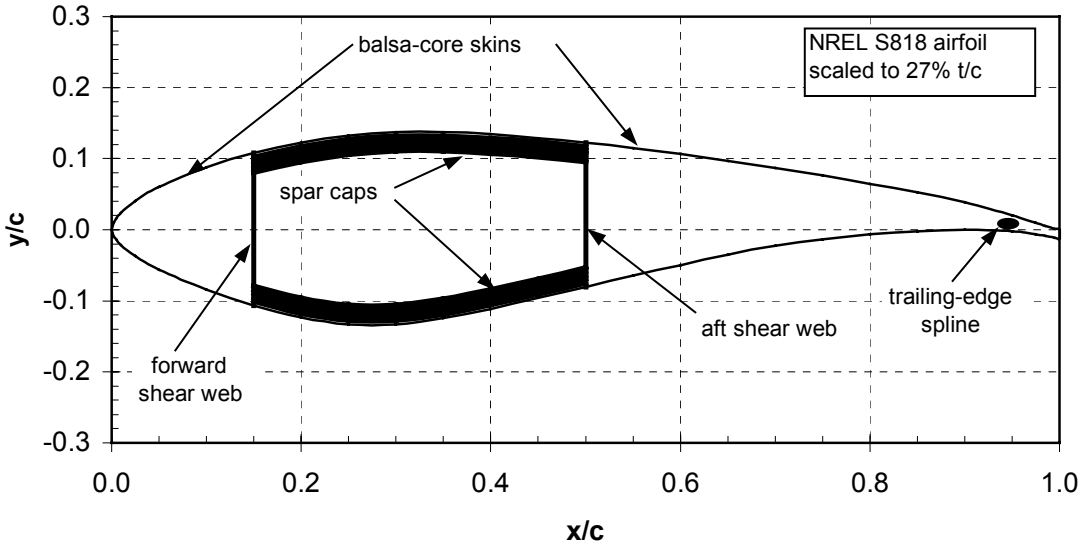

Figure 4. Arrangement of baseline structural model

As seen in the figure, the assumed placement of the shear webs results in a relatively wide spar. As a result, the spar cap material provides a significant contribution to the edgewise bending strength. Also note that due to the deep contour on the lower airfoil surface, the aft portion of the shear web will be less effective in flap bending than if it were concentrated in the deepest part of the foil (farther from the neutral bending axis). These aspects of the baseline structural configuration are addressed further in Section 4.2. Figure 4 also shows a "trailing-edge spline." This represents material added, as needed, for reinforcement in edge-bending strength.

Table 4 lists the layers in the baseline structural shell, and describes the material contained in each. The dimensions given in Table 4 were used in structural calculations for 750-kW rotor blades. The shear web cores (balsa) were assumed to be 1% c thick for all rotor sizes, however, the thickness of the shear-web skins (triaxial fiberglass) was increased for larger blade sizes.

Table 4. Structural-Shell Definition (750 kW)

Layer #	Material	Thickness
1	gel coat	0.51 mm
2	random mat	0.38 mm
3	triaxial fabric	0.89 mm
4 0%-15% c 15%-50% c 50%-85% c	 balsa spar cap mixture balsa	 0.5% c specified % t/c 1.0% c
5	triaxial fabric	0.89 mm

The skins and spar cap are E-glass/epoxy laminate. The triaxial fabric is designated CDB340, and has a 25%, 25%, and 50% distribution of +45°, -45°, and 0° fibers, respectively. The spar cap is composed of alternating layers of triaxial and uniaxial (A260) fabric. This stacking sequence results in spar cap laminate with 70% uniaxial and 30% off-axis fibers by weight.

Characteristic material properties for these lamina were derived based on a combination of test data and laminate theory calculations.[8,9] Table 5 summarizes the mass and stiffness properties for each material. Strength properties are addressed in Section 2.7.

Table 5. Summary of Material Properties

Property	A260	CDB340	Spar Cap Mixture	Random Mat	Balsa	Gel Coat	Fill Epoxy
E_x (GPa)	31.0	24.2	27.1	9.65	2.07	3.44	2.76
E_y (GPa)	7.59	8.97	8.35	9.65	2.07	3.44	2.76
G_{xy} (GPa)	3.52	4.97	4.70	3.86	0.14	1.38	1.10
ν_{xy}	0.31	0.39	0.37	0.30	0.22	0.3	0.3
υ_f	0.40	0.40	0.40	-	N/A	N/A	N/A
w_f	0.61	0.61	0.61	-	N/A	N/A	N/A
ρ (g/cm^3)	1.70	1.70	1.70	1.67	0.l44	1.23	1.15

Note that in performing the blade structural calculations, it was not required that the skin thickness and spar cap dimensions be integer multiples of the selected material lamina thickness. This was done to reduce the complexity of the calculations, and to avoid the need for step-jumps in the model definition and results. It was assumed that a suitable fabric (or combination of fabrics) could be identified that would be a near-match to the dimensions and fiber content modeled for each blade.

2.4 Calculation of Section Structural Properties

Once the baseline model parameters were established, a series of direct point-designs were performed, each design providing a "base case" for developing the computational modeling tool. Table 6 provides a summary of the preliminary structural base cases; the ratings indicated are related to the physical dimensions used for corresponding section analyses. As indicated by the table, the section mechanical properties were computed for each spanwise station using spar caps that were 0%, 5%, and 10% of the local maximum section thickness.

Table 6. Matrix of Structural Base Cases

Spanwise Stations	Airfoil t/c (%)	Spar Cap (% t)	Rating (MW)
25%	27	0, 5, 10	0.75
	27	0, 5, 10	5.0
	30	0, 5, 10	0.75
	33	0, 5, 10	0.75
	36	0, 5, 10	0.75
50%	24	0, 5, 10	0.75
	24	0, 5, 10	5.0
75%	21	0, 5, 10	0.75
	21	0, 5, 10	5.0
100%	16	0, 5, 10	0.75
	16	0, 5, 10	5.0

Second-order curves were then generated for mass per unit length, and bending stiffness (flapwise and edgewise) as a function of spar cap thickness. Figure 5 shows an example curve-fit to the flapwise bending stiffness (EI_{Flap}) for the 25% span blade station.

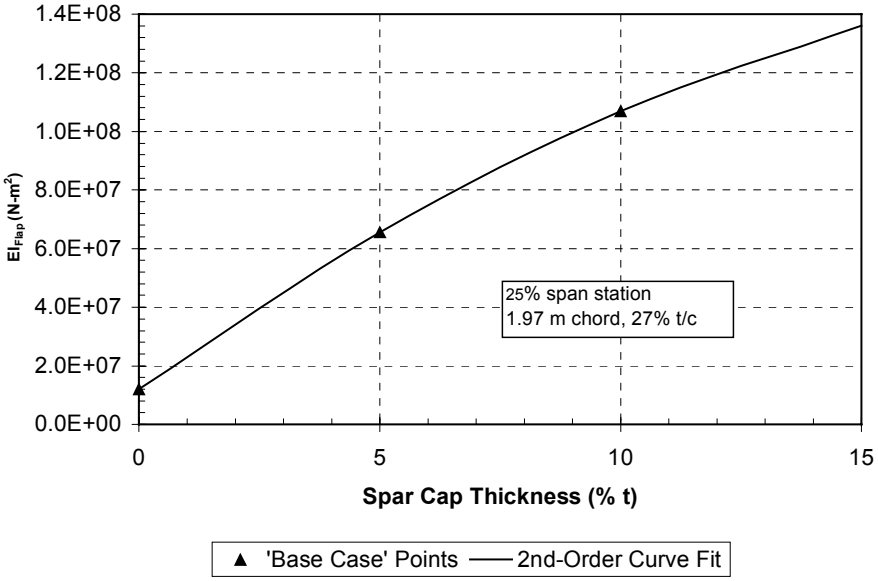

Figure 5. Example curve-fit of flapwise bending stiffness

An inverse curve-fit of the flapwise strength curves was then performed. With user-specified values of design load (flapwise bending moment) and design limits on material strain, the resulting curves allow calculation of the spar cap thickness required to support the given load.

To allow investigation of the blade thickness variations at the 25% r/R location, where the impact on mass and cost is the most significant, additional structural base cases were computed for airfoil shapes scaled to 30% and 36% t/c (as presented in the matrix of Table 6). These results were similarly fit with second-order curves as a function of spar cap thickness. A secondary curve-fit was then developed to allow modeling of variations in both spar cap thickness and airfoil section thickness at the 25% r/R station.

To provide accurate size scaling, structural base cases were also created for a blade size that represented a 5-MW turbine. By comparison to the 750-kW data, curve-fits were developed to model the substantial differences that were shown in the underlying base cases. In developing the 5-MW section models, the spar caps, skins, and shear webs were each treated independently, and scaled as appropriate. This treatment of the 5-MW base cases resulted in the designs departing from pure self-similarity as they scaled in size. For example, the gel coat and skin thickness did not increase in direct proportion to the blade chord.

An important clarification must be made in the use of "flapwise" and "edgewise" structural properties. Although the terminology of flapwise and edgewise is used throughout this work, the associated properties (calculated and used in the structural scaling model) are more properly termed "out-of-plane" and "in-plane," respectively. For each airfoil station, a twist angle was assumed, and the loads were applied and structural analyses performed in the rotated orientation. Figure 6 illustrates this approach for the 25% span station, for which the analyses were performed with a 10° rotation of the blade section. In determining the structural properties, moments were applied parallel to the original (untwisted) x-y axes. The structural-analysis code determines the location of the neutral axis for the rotated section, and calculates bending properties relative to those axes.

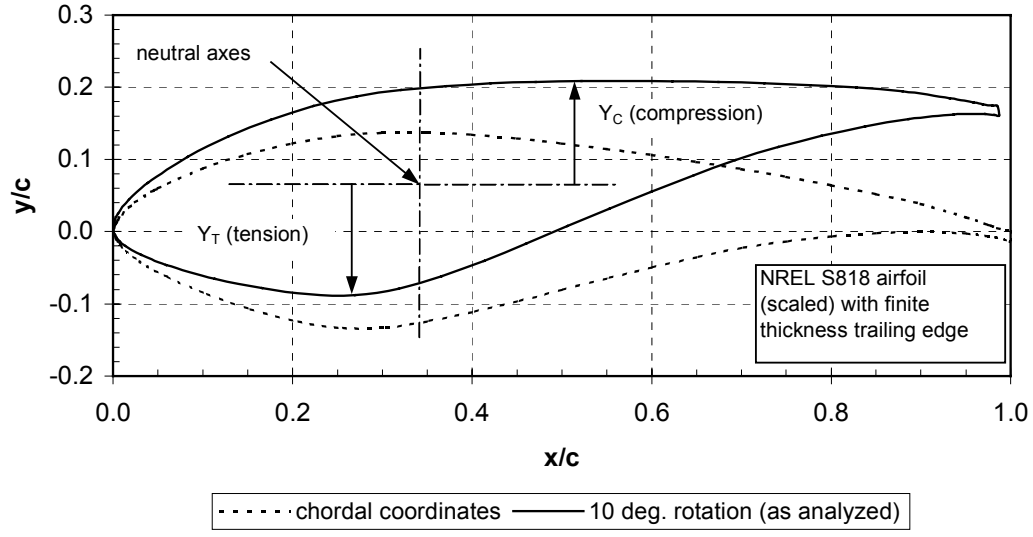

Figure 6. Orientation of blade section for "flapwise" and "edgewise" properties (used at 25% r/R for all rotor sizes)

As indicated in Figure 6, the critical fiber distances (tension and compression) are taken as the farthest material, in a perpendicular direction, from the out-of-plane neutral bending axis. Because of the rotated geometry, the critical tension and compression fibers will not occur at the same airfoil chord location, and will be separated by a vertical distance greater than the maximum airfoil thickness.

Although the approach taken adds some complexity to the analysis and subsequent interpretation, it is intended to realistically portray the loading condition for the blade in service. Table 7 summarizes the twist angles used at each section for the base case calculations, and also presents the near-optimal blade twist angles as determined by the PROPID aerodynamic code for two different values of design tip-speed ratio. The data indicate that the twist angles assumed for the structural analysis are a close approximation to the near-optimal blade twist. Also note that the distinction between the flap/edge and in/out-of-plane properties is the greatest at the 25% span station, and vanishes entirely at the 75% span station (where the twist is taken to be zero by definition).

Table 7. Summary of Blade Section Twist Angles (independent of rotor size)

Station (%R)	Assumed Twist (Deg.)	PROPID Near-Optimal Twist (deg.)	
		Design TSR = 7	Design TSR = 8
25	10	10.5	9.3
50	2.5	2.5	2.1
75	0.0	0.0	0.0
100	-0.5	-0.6	-0.4

2.5 Load Cases

After examining multiple different load cases to determine those which would likely govern the blade design, two primary load cases were selected for the purposes of developing structural designs. Peak bending loads were derived using a 50-year extreme gust of 70 m/s (IEC Class 1).[2] The gust was assumed to occur with the blades in a fully feathered position, with a ± 15° variation in wind direction. To simplify the loads development, it was assumed that this load case resulted in each blade section simultaneously reaching its local maximum-lift coefficient, and that the bending loads were entirely in the flapwise direction. The resulting loads were summed over the blade, to define characteristic peak bending moments at each blade station.

For edge bending, the designs were assumed to be governed by fatigue loading. A simplified loading spectrum was developed by combining the peak of gravity plus torque at rated power and assuming the loading is fully reversed. This load case was further simplified by assuming the rotor operated for 5000 hours per year at rated power, over a 20-year design life.

In addition to the two load cases described above, methods were investigated for defining a simplified flap-fatigue spectrum. However, no suitable flap fatigue model was identified that had the combination of reliability and computational simplicity desired for this scaling study.

2.6 Partial Safety Factors

Per the IEC 61400-1 standard, a series of partial safety factors must be used to adjust from "characteristic" to "design" values of material properties and loads. To be consistent with other WindPACT studies, the original intent for this project was to use IEC partial safety factors throughout. However, it was found that IEC did not always provide sufficient guidance in the selection of factors. Specifically, the IEC 61400-1 requires a "general" material factor of 1.1. The IEC standard further states that material factors will be applied to account for "…scale effects, tolerances degradation due to external actions, i.e., ultraviolet radiation, humidity and defects that would not normally be detected"; however, the IEC document provides no specific guidance on appropriate values for these additional factors. Conversely, the Germanischer Lloyd (GL) standard provides an explicit list of partial safety factors for composite materials.[10] For a static-strength evaluation of glass-reinforced plastic, the GL factors are:

γ_{M0} = 1.35 (general material factor)
C_{2a} = 1.50 (influence of aging)
C_{3a} = 1.10 (temperature effect)
C_{4a} = 1.20 (hand lay-up laminate)
C_{5a} = 1.10 (non-post-cured laminate)

The GL standard further states that γ_{M0} is to be used in all cases, but that the C_{ia} may be adjusted if demonstrated by experimental verification. Applying the GL factors as specified implies a combined material factor of 2.94 for static-strength analyses. For fatigue verification, the GL standard states that the same partial material factors will be used, with the exception of the 1.5 factor for "aging." In the absence of IEC guidance in this area, the GL material factors were used for these scaling-study calculations.

The GL partial load factor for an extreme 50-year event is 1.50, whereas the corresponding IEC load factor is 1.35. The IEC load factor of 1.35 was chosen for these scaling-study calculations.

2.7 Material Design Strength

Strain-based characteristic-strength values were derived for the baseline E-glass/epoxy laminate using a combination of test data and laminate theory.[8,9,11] As described in the previous section, partial material factors were developed based on the values specified by GL. For static calculations, a combined material factor of 2.9 was typically used. For fatigue calculations, the material partial safety factor was 2.9/1.5 = 1.93. Table 8 summarizes the values for characteristic and design laminate strength that were used to develop the baseline blade designs.

Table 8. Design Values for Laminate Strength

	Strength (με)		
Loading	**Characteristic**	**Design (static)**	**Design (fatigue, single cycle)**
Tension	22,000	7586	11,379
Compression	10,500	3620	5431

For fully reversed loading, a fatigue curve was developed of the form:[11]

$$\frac{\varepsilon}{\varepsilon_o} = 1.0 \cdot N^{-1/m} \qquad \text{(Eqn. 6)}$$

where

ε_o ≡ single-cycle design fatigue strain for compression
N ≡ number of loading cycles
m ≡ 13.

2.8 Full-Blade Calculation

A full-blade calculation ties together all the model elements described above. User input to the spreadsheet-based calculation includes:

1) Rotor radius and rated power.
2) Chord dimensions and flapwise design bending moments at 25%, 50%, and 75% span stations.
3) Diameter and design bending loads for the circular root connection.
4) Diameter of root studs and factors for scaling of laminate required for root/stud interface.
5) Factor to account for "parasitic" mass due to excess material and bonds.
6) Design values for peak laminate strain, and ε-N parameters for the edge-bending fatigue calculation.

The following sections provide a summary of the process used in a full-blade calculation.

2.8.1 Root Design

For the purposes of this study, a circular root bolt pattern was assumed. As indicated by Figures 7 and 8, several root design parameters were inferred from commercial blade designs.[1] Although root connection bolts are available in discrete size increments, the scaling calculations use continuous non-integer functions to model the root connection and associated mass. The laminate at the root is sized according to stud-bonding requirements, with user-input scaling parameters. Preliminary calculations showed that typical commercial root designs exceed the strength requirement implied by quasi-static strength verification, so the empirical (conservative) relationships were used throughout the study to determine root designs.

To minimize the impact of the root-design assumptions on the total calculated blade mass and cost, a second calculation is performed near the root, where the required blade structure is determined on the basis of the design loads. This "inboard root design" calculation is described in the following section.

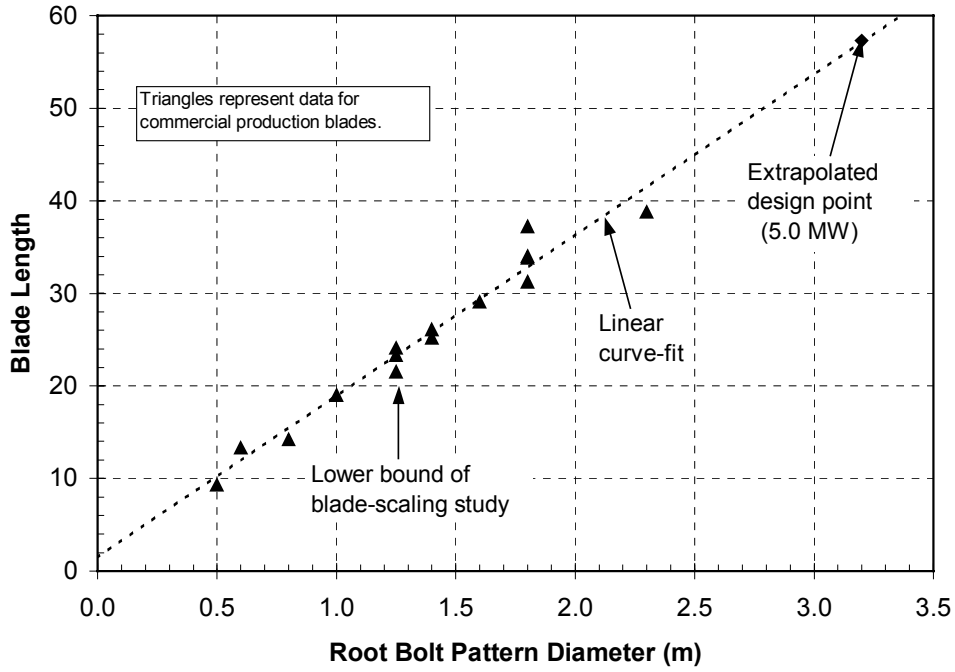

Figure 7. Root-sizing trend from commercial blade designs

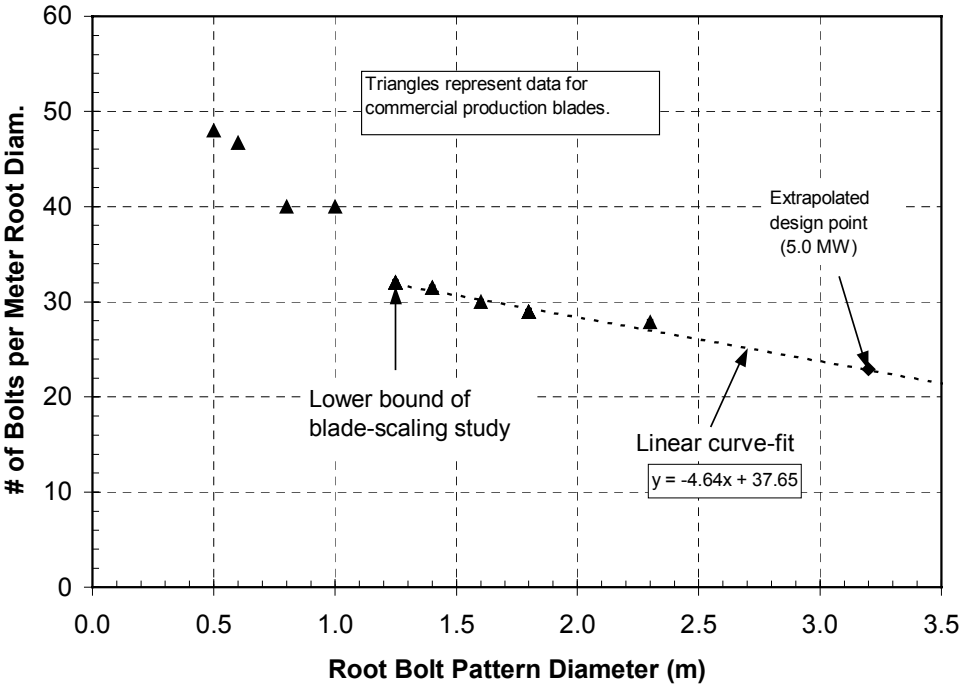

Figure 8. Bolted-joint trend from commercial blade designs

2.8.2 Inboard Root Section

The buildup of laminate required for stud bonding is assumed to taper away within a user-specified distance from the root. The typical assumption used was that the drop-off of excess laminate occurs within a distance of 2% R from the root plane. It is further assumed that the blade cross section at this station remains circular, and is composed of a thick-laminate shell with the same composition as the spar cap material. Shell thickness at this station is determined by bending-strength requirements, based on a direct calculation within the structural design spreadsheet.

2.8.3 Remaining Blade Stations

At 25%, 50% and 75% span, the blade section structure is determined using the design bending loads and material strain limits. However, rather than using a direct calculation, the input is used in an inverse-process (via the curve-fits described in Section 2.4) to determine the spar cap thickness required to meet the design criteria. Once the spar cap has been sized according to the design load, section structural properties (EI_{Flap}, EI_{Edge} and mass per unit length) are directly calculated at each section based on chord length and spar cap thickness.

The design bending moments necessarily vanish at the tip section. Here, the blade section properties are calculated based only on chord, with the assumption that the spar cap has entirely tapered away.

Following the initial structural sizing of the blade, additional verifications and/or adjustments are performed:

1) Fatigue life is verified for edgewise bending, assuming 5000 hours per year for a 20-year design life at an assumed constant-amplitude loading. If 20-year fatigue life is not achieved, then additional structure is added at 95% span (trailing-edge spline) until the edge-fatigue criterion is met.
2) Tip deflections are calculated for the 50-year extreme loads. For the purposes of this work, a guideline was used that the maximum tip deflection should not exceed 10% of the rotor radius. However, this guideline was not used to determine the required blade structure; rather it was used to comparatively assess blade design variations.
3) The option for a constant multiplier on the blade section mass is included to account for "parasitic" mass due to bonding material and inevitable inefficiencies in material usage. For this report, the parasitic-mass adjustment was assumed to be a constant 10% of the total blade mass. In commercial practice, the amount of non-structural material in a blade will be determined by a trade-off between labor and material costs. Although the manufacturing economics at large scales are likely to favor additional labor expenditures to save material, no attempt was made in this study to quantify that effect.

Table 9 provides an example of the model output for a 750-kW blade with a design tip-speed ratio of 7 and a maximum chord of 9% R. Moving from the root towards the tip section, the values for EI_{Flap} show a decline that is approximately exponential; the mass decline is approximately linear from the 25% span station outward. For each design, the total blade mass is calculated by a summation over the entire span, assuming a linear variation in unit mass between stations.

In the absence of a parasitic-mass adjustment, each calculated mass is a theoretical minimum for the configuration and materials modeled; in practice, other design considerations such as flap fatigue, damage tolerance, and/or load paths requirements may result in higher mass values.

Table 9. Output from Full-Blade Calculation (750-kW Rotor at TSR_{Design} = 7, c_{max} = 9% R)

Blade Station		Spar Cap	Section EI (N-m^2)		Mass
r/R (%)	(m)	Thickness (% t)	Flap	Edge	(kg/m)
5	1.2	N/A	1.91E+09	1.91E+09	662.4
7	1.6	N/A	3.13E+08	3.13E+08	109.8
25	5.8	4.97	8.41E+07	2.12E+08	116.0
50	11.6	5.92	1.90E+07	7.48E+07	69.3
75	17.5	5.45	2.14E+06	1.54E+07	28.4
100	23.3	0.0	3.48E+04	1.18E+06	5.7

Blade structure =	1577 kg
Root connection =	111 kg
Total blade =	**1688 kg**

2.9 Cost Modeling

Cost functions were developed, based on current industry experience, for blade masters, mold sets, tooling, and production blades.[12] The cost models assume the baseline structural configuration and materials as described above.

Costs for master blades and mold sets scale approximately as the blade surface area, with the cost per square meter depending on the tolerances required. Tooling also scales with the blade area, but carries an additional cost escalation due to reinforcement requirements as blade sizes increase. The cost functions used for these items are:

$$\text{Master and molds}\,(\$) = 1880 \cdot S \qquad \text{(Eqn. 7)}$$

$$\text{Tooling}\,(\$) = 4300 \cdot \left(\frac{R}{35\,\text{m}}\right)^{0.5} \cdot S \qquad \text{(Eqn. 8)}$$

where

S ≡ total blade surface area (m^2).

For a mature process, production costs (material and labor) are directly proportional to the blade mass. However, there is a "learning curve" required to develop a mature process. The learning curve is cycle-dominated, and will require approximately 100 cycles before the long-term production rate is realized. A mature production cost of $10.45 /kg blade mass was used for this study. However, the production costs were escalated according to the schedule of Table 10 to account for process development.

Table 10. Cost Multipliers for Developing Mature Production Process

Blade Quantity	Multiplier on Production Cost
1–20	4.0
21–60	1.5
61–100	1.15

Complete cost results are given in Section 4.5, where it is shown that the process learning curve has a meaningful effect on blade costs for the range of rotor sizes considered. A production rate of 200 MW per year implies 800 blades at 750 kW, but only 120 blades at 5 MW. Therefore, the cost penalty for initial production cycles has an increasing impact on the first-year production costs as rotor sizes increase, and a complete cost assessment depends on both annual production rates and the extent (number of years) of sustained production.

Relationships for bonded-stud geometry, mass, and cost were developed. The cost function used for the bonded studs is $20/kg of stud material.

3. Evaluation of Aerodynamic Designs

The selection of blade airfoils and the development of their aerodynamic properties is described in Section 2.2. With those design parameters fixed, the remaining aerodynamic-design variables are the planform (chord schedule) and twist distribution. PROPID calculations were performed for a wide range of ratings and design tip-speed ratios (TSR_{Design}). The design tip-speed ratio is the tip-speed ratio at which optimum aerodynamic performance (C_{Pmax}) is realized, and during variable-speed operation to rotor speed will be controlled to maintain the TSR_{Design} until either the maximum allowable blade tip speed or the maximum system power point is reached.

The calculation procedure used for the aerodynamic designs is generally the same as that described in Reference 13. For each design, the PROPID calculations were used to determine a near-optimal planform and twist schedule. Figure 9 shows near-optimal planforms, as determined using PROPID, for blades with design tip-speed ratios of 7 and 8. When described in non-dimensional terms, the near-optimal blade shapes were found to be independent of rotor size in the 750 kW to 5 MW range. Both planforms are nearly linear in the outboard region, with a pronounced flare in the chord distribution near 25% span.

The planform will effect both the aerodynamic and structural properties, with the inner portion of the blade having the largest effect on structural mass. As seen in Figure 9, the near-optimal chord size in the outer region of the blade is strongly dependent on the design tip-speed ratio, with a higher tip-speed ratio favoring a more slender planform. However, in the inboard region of the blade, the chord schedule will have a relatively small effect on the aerodynamic performance.

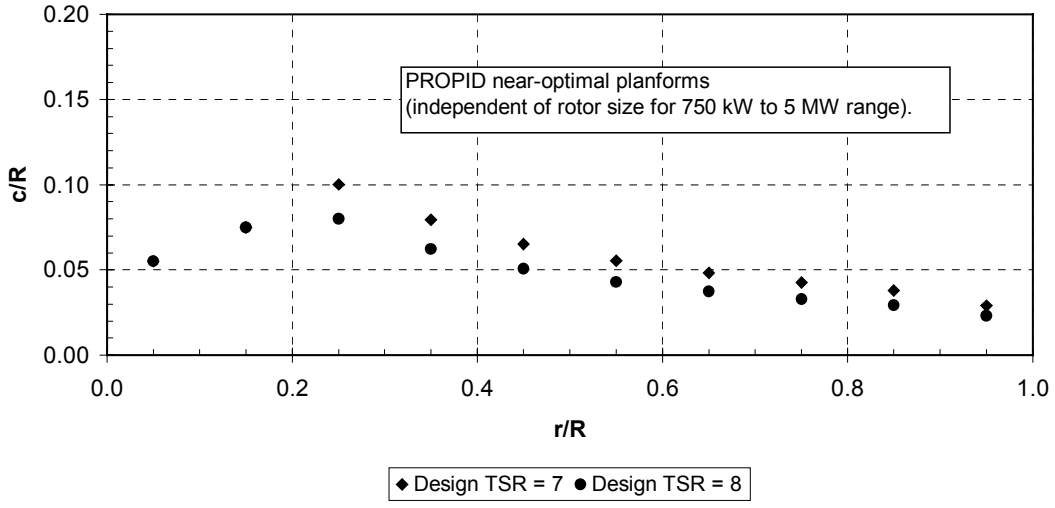

Figure 9. Near-optimal blade planform for design tip-speed ratios of 7 and 8

The majority of commercial blade designs have a linear- or near-linear taper in planform from the tip to the maximum chord location. Although the aerodynamic and structural performance will theoretically improve for blades with a planform that flares toward the maximum chord, the observed trend for commercial blades reflects the facts that; (1) the aerodynamic performance gains from large inboard chord dimensions are small, (2) significant non-linearity in the planform adds cost and complexity to the blade manufacturing, and (3) increased chord inboard is not the

most effective way to improve structural performance in flap bending, which governs most current blade designs.

To systematically investigate the effect of planform variations on aerodynamic and structural performance, a series of linear planforms was constructed. The choice of an identically linear planform is one of computational convenience; similar trends concerning the trade-off between aerodynamic and structural performance would be found for blade designs that have slight-to-moderate deviations from a linear planform. At the 75% span station, each planform was constrained to pass through the original PROPID chord point, and a varying schedule of c_{max} was specified at 25% span. Figure 10 shows a resulting family of linear planforms, where c_{max}/R is varied between 6% and 10%, in 1% increments. By inspection, it can be seen that small values of c_{max} result in the best fit of the PROPID points for the outer 50% of the blade. The linear planform with c_{max} = 7% R (shown as a dashed line in Figure 10) is a particularly good match to the PROPID data points for the outer blade.

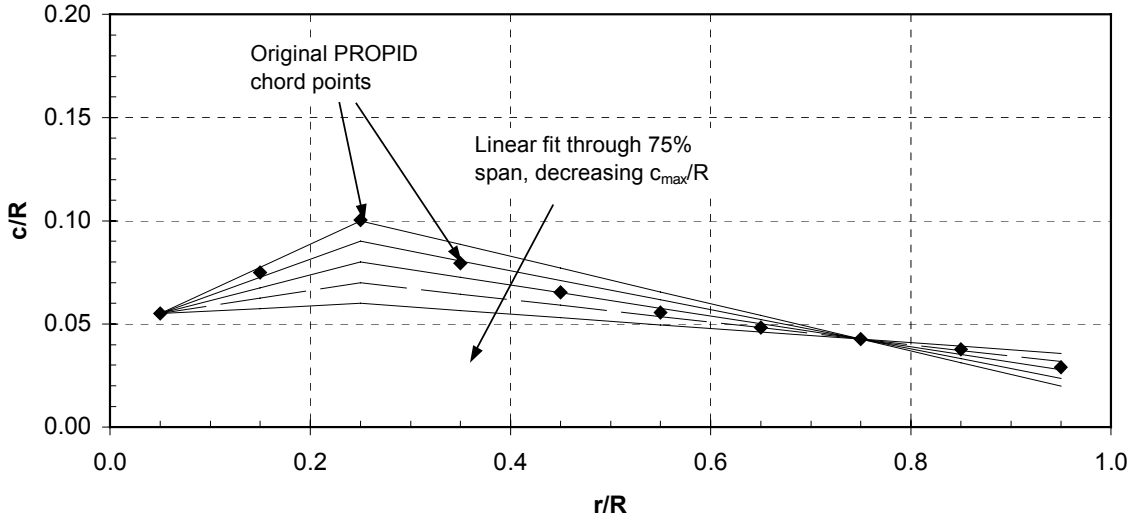

Figure 10. PROPID near-optimal planform (at TSR_{Design} = 7), with linear variations

Planform families were similarly developed for a range of design tip-speed ratios, and each design analyzed for C_P-TSR and C_{Pmax}. In all cases, the PROPID near-optimal twist distribution was used in the analyses. Figure 11 shows a plot of the resulting C_{Pmax} variation with c_{max}. For design tip-speed ratios of 6 and 7, the C_{Pmax} curves are relatively flat. Consistent with the trends seen in Figure 10, the TSR_{Design} = 7 curve shows a flat optimum at c_{max} = 7% R. The TSR_{Design} = 8 curve is significantly steeper, and favors small values of c_{max}.

In addition to C_{Pmax}, energy production from a variable-speed, active power control turbine will depend on the entire C_P-TSR curve and other parameters such as maximum tip speed, rotor diameter, air density, hub-height wind speed distribution, drivetrain efficiency, and turbine availability. Complete calculations of power performance and energy production will be presented in Section 4.4. For this discussion, the C_{Pmax} for each design will be used as an indicator of aerodynamic performance.

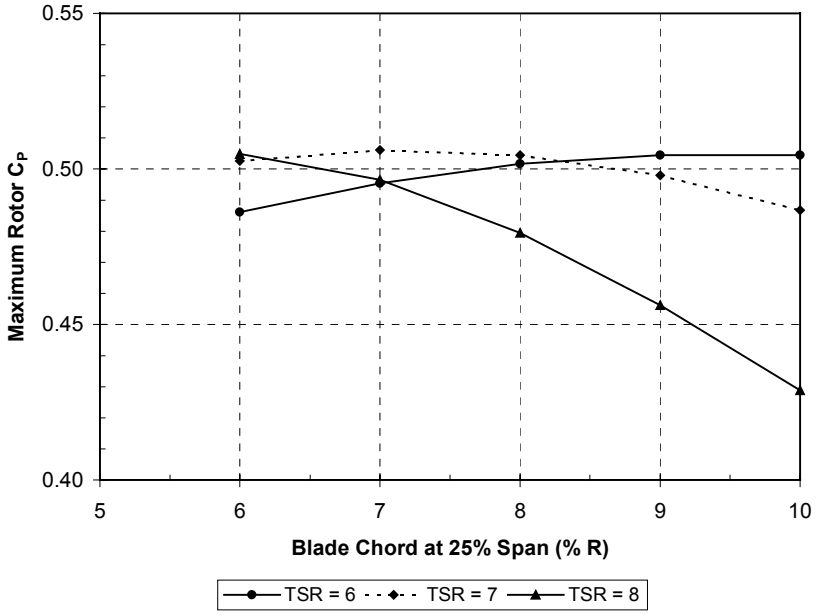

Figure 11. Effect of planform variations on rotor C_{Pmax}

To investigate the structural implications of these planform variations, a matrix of blade structural designs was developed. Design output is given in Table 11, with a summary of both aerodynamic and structural properties. The results shown in the table illustrate several trends concerning the trade-off between efficient aerodynamic and structural design. Although the designs were performed for a 750-kW rating (with diameter fixed at 23.3 m), the indicated trends generalize to larger rotor designs.

Table 11. Summary of Blade Designs at 750-kW Rating

Design TSR	C_{max} (% R)	C_{Pmax}	Solidity (%)	Blade Mass (kg)	Spar Cap Thickness (% t)		Max. Tip Deflection (% R)
					at 25% R	at 75% R	
7	10	0.487	5.84	1582	3.2	4.5	11.9
7	9	0.498	5.56	1688	5.0	5.4	12.4
7	8	0.504	5.28	1852	8.3	6.5	13.1
7	7	0.506	5.01	2120	15.0*	13.6*	14.3
8	9	0.456	5.04	1347	3.4	6.6	14.0
8	8	0.480	4.76	1469	5.6	9.0	14.6
8	7	0.496	4.49	1664	10.2	11.6	15.7
8	6	0.505	4.21	2013	20.1*	14.4*	18.4

***** Spar caps above 12% exceed the bounds of high-confidence curve fitting.

For both $TSR_{Design} = 7$ and $TSR_{Design} = 8$, a general trend of increasing mass with decreasing c_{max} is seen. This is not surprising. With a fixed t/c at the 25% span station, shorter chord lengths mean that the physical blade thickness is also decreasing, resulting in less efficient structural sections. This trend is also apparent in the spar cap thickness. At 25% r/R, a near-doubling of required spar cap is seen with each 1% decrease in c_{max}/R. This trend is the result of two compounding effects: (1) the thickness of the structural section is decreasing, and (2) as spar caps become thicker, new material is placed further towards the shell interior (closer to the neutral bending axis).

The aerodynamic performance trends run contrary to those for structural properties. The best (linear) fit to the near-optimal chord distribution favors narrow inboard chords, and C_{Pmax} increases as c_{max} decreases. For both TSR_{Design} = 7 and 8, blades which are slender enough to reach the optimal C_{Pmax} are also relatively heavy due to the structural inefficiency discussed above.

Given the same value of c_{max}, the tip deflections increase with increasing design tip-speed ratio. This is because the blade structure has been determined on the basis of design strain values for the laminate. Increasing TSR_{Design} results in a more slender outboard planform, and the thickness of the blade sections decreases accordingly. Maintaining a constant value of strain in the outer laminate will therefore result in greater curvature and higher deflections.

Between mass, aerodynamic performance, and tip deflections, it is difficult to find a suitable design combination for TSR_{Design} = 8. As an example, at c_{max} = 8% R, the blade designed for TSR_{Design} = 8 has a relatively low mass of 1469 kg, and an acceptable C_{Pmax} of 0.48. However, this design also has a relatively high tip deflection of 14.6% R. If additional structure is added to reduce the tip deflection by 2.2% R (i.e., to match the deflection of the TSR_{Design} = 7, c_{max} = 9% R design), the blade mass would increase by 15% to 1694 kg. A review of the data in Table 11 shows that moving to higher or lower values of c_{max} at TSR_{Design} = 8 results in either a significant increase in mass and deflection or a rapid decrease in aerodynamic performance. This trend clearly illustrates the challenge of designing efficient blades at high TSR_{Design} using the baseline configuration and fiberglass/epoxy materials.

At TSR_{Design} = 7, the blade with c_{max} = 9% R is a good compromise between mass, C_{Pmax} and stiffness. As such, this planform was selected as the baseline aerodynamic design for the remainder of this scaling study. In making this selection, trends in commercial designs were reviewed. Figure 12 shows a plot of c_{max}/R for current commercial designs.[1] Although there is significant scatter, there appears to be a trend towards decreasing c_{max}/R as rotors sizes increase. Among other factors, this may be due to size considerations in handling and transportation costs, issues which will be of increasing importance as rotors continue to grow in size. However, as the data of Table 11 indicate, restraining maximum chord size will come at the expense of increased mass or other modifications to the design and/or materials.

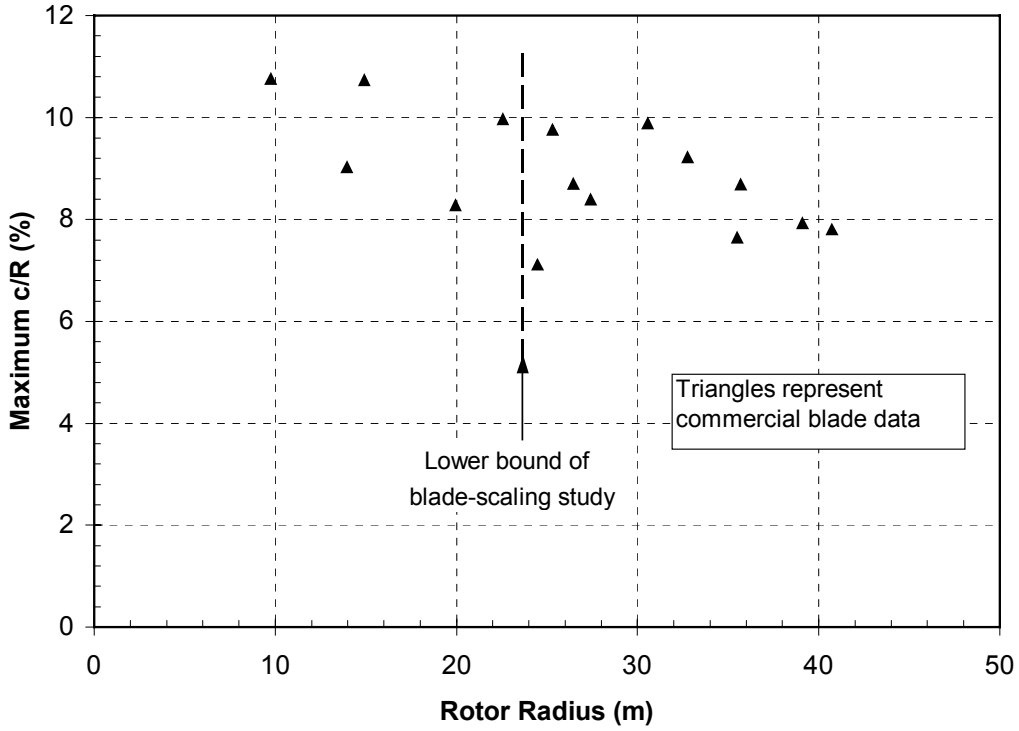

Figure 12. Maximum chord size for commercial blade designs

4. Scaling Results

4.1 Initial Scaling of Baseline Design

Using the aerodynamic design identified in the previous section, blade structures were modeled for the range of 750 kW to 5 MW.

4.1.1 Edgewise Fatigue Considerations

The ratio of gravity to torque load for the baseline blade design is plotted in Figure 13, which shows an increasing contribution of gravity loads to the total edge-bending moment as rotors become larger. Figure 13 also shows the edge fatigue "capacity," which is the ratio of actual edge-fatigue strength to that required for 20-year life under the assumed loading. For the blade modeled, the edge-fatigue capacity drops below unity just above R = 55 m, which corresponds to a rotor of approximately 4 MW.

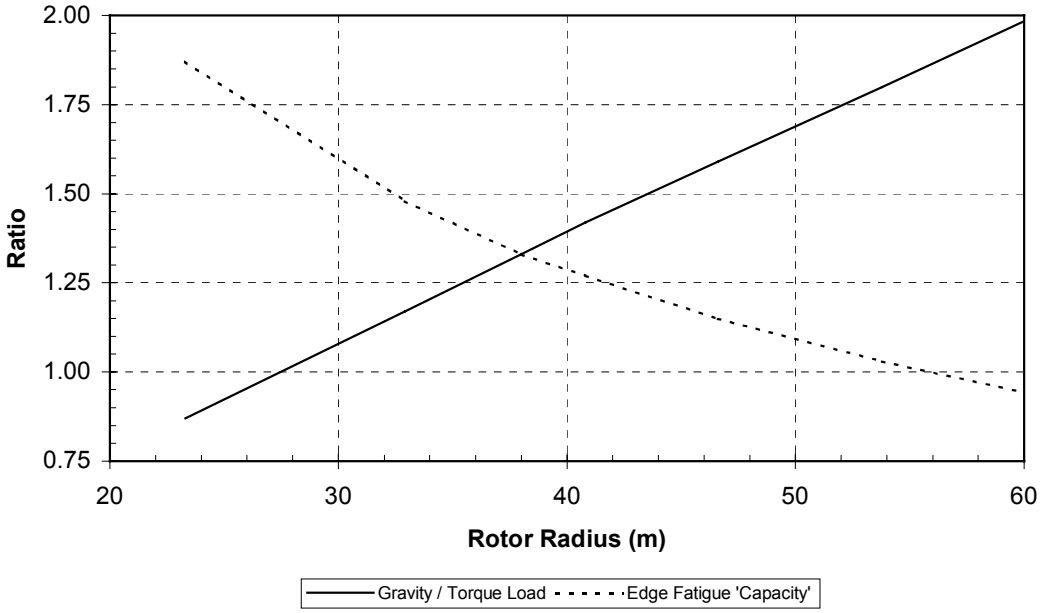

Figure 13. Gravity effects on blade edge-bending loads and fatigue strength

The absolute point at which the blades become edge-critical must be understood within the context of the blade configuration modeled. The choice of c_{max} = 9% R results in significant edge-bending capability relative to planforms with smaller inboard chord size. In similar fashion, the assumption of spar cap location (from 15% to 50% chord) also favors edge-bending strength. For a different planform and/or internal configuration, the general trend shown in Figure 13 would still hold, but the size at which blades become edge-critical would shift.

Although edge-bending calculations were performed along the entire blade, the only station at which edge-fatigue loading exceeded the section capability was at 25% span. When this occurs,

a secondary calculation is performed to determine how much additional material must be added at 95% chord to match the loading requirement. This calculation of trailing edge spline was automated within the spreadsheet-based modeling tool, and the blade scaling results presented herein contain mass contributions due to edge reinforcement (as needed).

4.1.2 Comparison with Commercial Blade Masses

Figure 14 presents a comparison of scaling-model results with available mass data for current commercial blades.[1] The solid line represents modeling calculations for the baseline blade configuration (t/c = 27% at c_{max}).

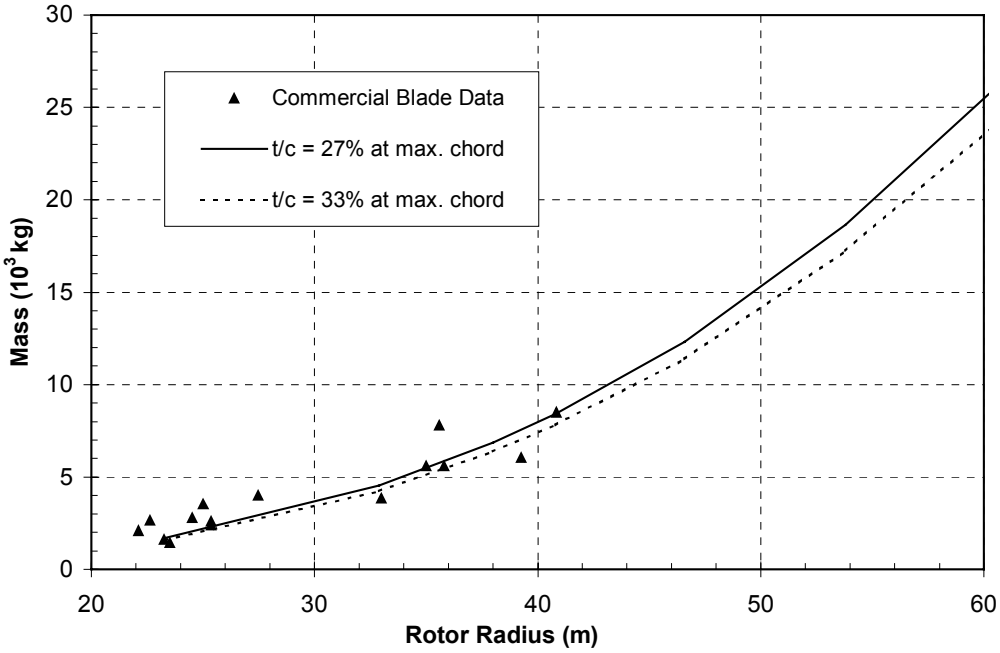

Figure 14. Comparison of modeled mass with commercial blade data

The modeled blade mass scales as approximately $R^{2.9}$ over the range between 23 and 60 m. For pure similarity-scaling of a given blade structure, the mass would grow as a cubic of radius. However, in these calculations, the scaling of blade skins was treated independently of the structural spar, resulting in the lower mass-growth exponent. The general modeling trend depicted in Figure 14 held throughout this study—for a fixed set of design conditions (loads, planform, section thickness distribution, and materials), the calculated blade mass scaled as a 2.9 exponent over the range of interest.

The commercial blade data in Figure 14 show significant scatter; however, the average mass values scale approximately as $R^{2.4}$ over the range between 23 and 40 m. This discrepancy between the commercial blade trend and the 2.9 exponent of the modeling results is apparent in the comparisons shown in Figure 14. At the low end of the scaling range, the modeled results (solid line) fall at the lower bound of the commercial blade mass data. However, at the largest rotor sizes, the modeled results begin to overshoot the commercial blade masses.

After reviewing these results, it was concluded that the structural-scaling model is accurately characterizing the mass growth for scaling up a fixed-blade design, and that the lower mass-scaling exponent implied by the commercial blade data embodies significant design evolution over the range considered. In the following sections, the structural-modeling tool is used to investigate variations on the baseline blade design, to quantify the mass reductions possible, and to identify practical limits to mass reduction from each modification.

4.2 Parametric Variations on Baseline Blade Design

4.2.1 Design Wind Speed Class

Assuming that overall design is held fixed (same airfoils, chord and thickness distribution, structural layout and materials), the blade structural mass is directly proportional to the design load. For the current study, the defining bending loads are proportional to the square of the design (extreme gust) wind speed. If the design criterion was shifted from Class 1 to Class 2, and assuming that the extreme wind load still governed the design, the blade mass would scale as $(70/59.5)^2$, or a 38% reduction.

The actual wind speed design criteria were not available for the complete set of commercial blade masses shown in Figure 14. However, the majority of blades shown appear to have been designed for Class 1 or a near equivalent. As such, all structural calculations presented in this report have been based on Class 1 design conditions.

4.2.2 Thickness Distribution

As discussed previously, for a given airfoil t/c, increased chord will also increase the physical thickness and the structural efficiency of the section. A more direct way to improve the flap-bending efficiency of a section is to increase t/c. Again, structural efficiency is competing with aerodynamic considerations, which favor thin airfoils. However, as rotors become larger, Reynolds number effects may allow the use of thicker airfoils, while still maintaining desirable aerodynamic performance.

The effect of increasing thickness on blade mass is illustrated in Figure 14, where the dashed line indicates calculated blade masses for the baseline blade with the thickness at c_{max} increased to t/c = 33%. The figure indicates a significant decrease in blade mass for the thicker inboard section, and the agreement between the commercial blade data and the calculated results is improved in the 35-to-40 meter range.

Figure 15 plots the fractional decrease in total blade mass as a function of t/c at maximum chord. The figure shows that significant mass reductions may be realized by increasing the section above 27%, but that the mass reduction increments diminish with increasing values of t/c.

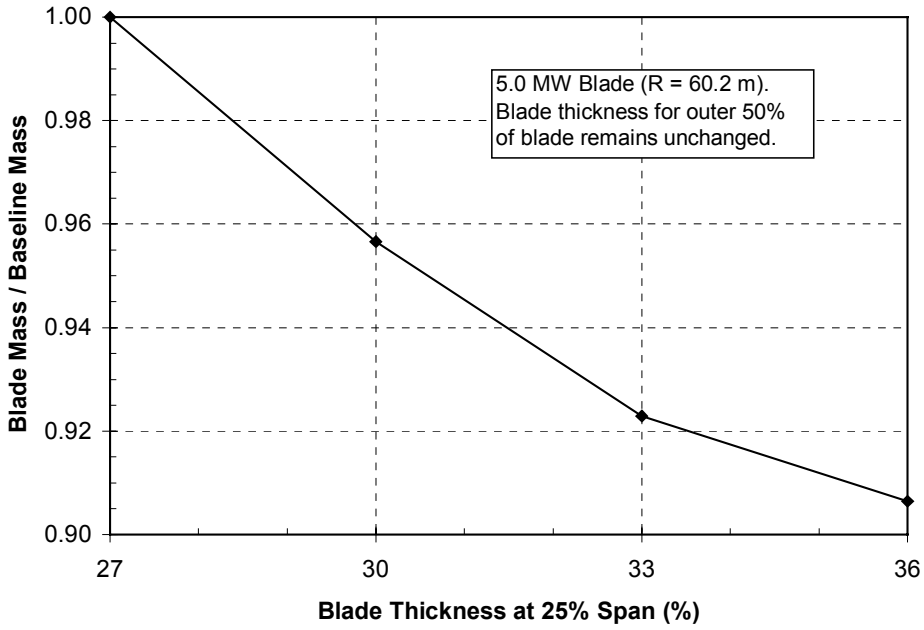

Figure 15. Effect of inboard airfoil t/c on total blade mass

Airfoil design is integral to realizing the desired aerodynamic performance from thicker airfoil sections. Unfortunately, airfoil design and analysis codes have difficulty modeling the aerodynamic behavior of such sections. Wind tunnel data, and ultimately field-test results, will be required to determine the extent to which airfoil thickness can be increased in large wind turbine applications. However, there will clearly be a practical limit to maintaining efficient aerodynamic performance.

4.2.3 Material Partial Safety Factors

The blade mass will be directly proportional to the partial safety factors applied to the design. Therefore, if a 10% reduction in material factors can be justified (i.e., by increased confidence due to material testing), then that would result in a 10% decrease in blade mass. However, allowing a lower factor on the material properties is equivalent to allowing higher strain values at the design load, and for a given blade shape the maximum tip deflections would increase by the same proportion.

As shown in the earlier analyses (see Table 11), the blade designs under consideration already exceed the estimated maximum deflection of 10% R. This criterion was not rigorously developed, but is considered a realistic estimate of deflection limits for common turbine configurations. The implication of the modeling results is that the blade designs under consideration are near a crossover point where they become stiffness governed. As such, the mass reductions possible purely by a reduction in material factors (for the baseline composite materials and structural configuration) would be constrained.

4.2.4 Spar Cap Composition and Arrangement

The baseline spar cap modeled in this study is composed of 70% unidirectional and 30% off-axis fibers (by mass), spanning from 15% to 50% chord, with constant thickness. To investigate the effect of these assumptions on the calculated blade masses, parametric analyses were performed for the 25% r/R blade section. The results of these parametric studies are summarized in Table 12.

Table 12. Parametric Analysis of Spar Design

	Mass Reduction (%)	
Case	**5% thick spar cap**	**10% thick spar cap**
Increased 0° fibers	3.5	4.7
Shift spar material	2.2	3.3

The first parametric analysis considered a stacking sequence of two layers of uniaxial A260 fabric for each layer of triaxial CBD340, resulting in a modified spar cap composition of 80% unidirectional and 20% off-axis fibers. An iterative structural calculation was performed to determine the amount of spar cap material required to achieve bending strength equal to the baseline section.

Table 12 shows the mass reductions achieved by this modification, at 5% and 10% (original section) spar cap thickness. For a section with large spar caps, the 10% increase in unidirectional fibers results in a mass reduction of 4.7%. As a percentage of section mass, this result would be of similar magnitude at all blade stations. This modification would also have a negligible effect on edgewise-bending capability. However, off-axis fibers are needed in the spar cap to inhibit crack propagation. Designers may generally consider a 70%-to-30% mixture of on- and off-axis fibers as appropriate; although the unidirectional content may be increased somewhat, robust-design considerations will dictate a practical limit.

The second parametric analysis performed for the 25% r/R section concerns the location of the spar cap material within the blade shell. The baseline section design assumes constant-thickness spar caps spanning between 15% and 50% chord. Inspection of Figure 4 shows that (for flap bending) a more structurally efficient structure would be realized by a tapered spar cap, with maximum thickness in the deepest part of the blade contour, and diminishing thickness towards the shear webs.

Analyses were performed to evaluate the effect of tapered spar caps, again using iteration to match the baseline bending strength. Table 12 shows that for thick spar caps, a 3.3% mass reduction may be realized for the 25% blade station. Although concentrating the spar cap material in the deepest part of the foil will increase the structural efficiency in flap bending, it will, however, reduce the capability in edge bending. For the case indicated in Table 12 (10% spar cap), tapered spar caps resulted in a 12% reduction in edge-bending strength. Therefore, the trade-off between flap- and edge-bending capability must be evaluated (along with manufacturing considerations) in determining the optimal location of spar cap material. Also, the outboard airfoils have less section curvature than the 25% blade station, and as such, the percentage mass reductions possible from the use of tapered spar caps would decrease in the outer portions of the blade.

4.3 Discussion of Scaling Results

Of the variations on the baseline design, the greatest reductions would be realized by the use of a lower design wind speed class. However, this decision depends primarily on markets targeted by the manufacturer, and it is expected that Class 1 design regimes will continue to be of interest for large wind turbines.

A reduction in material partial safety factors can also lead to significant mass reductions, but require justification by laminate and/or blade tests, and result in larger tip deflections under design load conditions. Modeled results indicate that (at minimum mass) the baseline blade designs are near to the point of being stiffness governed. As rotors grow in size and mass, there will be additional motivation to decrease rotor overhang. This will, in turn, reduce the magnitude of allowable tip deflections, and constrain the mass reductions made possible by reduced partial material factors.

Increasing the blade section t/c was shown to significantly reduce mass. For large turbines, Reynolds number effects increase the thickness for which airfoils will maintain efficient aerodynamic performance. Due to the limitations of aerodynamic analysis codes, the extent to which the thickness envelope may be pushed will likely require near-scale or full-scale field testing to determine. However, there will clearly be a practical limit to economic mass reductions from increasing section thickness.

It was shown that the spar cap composition and details of the material placement can result in mass reductions that are meaningful, but more subtle than the effects discussed above. Mass reductions due to increased unidirectional fiber content must be balanced against considerations of structural robustness, and the placement of the spar cap material within the section contour requires a trade-off between flap- and edge-bending strength requirements.

Recalling Figure 14, the masses modeled for blades with 33% t/c at maximum chord showed good agreement with data for commercial blades in the 35-to-40 m range. At this point, it is important to recognize that:

1. In the absence of an adjustment for parasitic mass, the current method calculates the theoretical minimum mass for the blade design modeled—any other considerations, such as load path requirements, damage tolerance, and flap fatigue can only increase the masses above those modeled.
2. The extent to which actual blade designs carry parasitic mass depends on a trade-off between labor and material costs, and will vary somewhat from manufacturer to manufacturer. The 10% adjustment for parasitic mass applied to the results presented herein is considered to be a good approximation to blade-manufacturing reality for the hand lay-up process under consideration. Although the economics of large blades may shift the emphasis towards saving material, there will be a practical limit to minimizing the parasitic mass.
3. All of the blade scaling results shown were generated for a maximum chord of 9% R. This is towards the upper end of c_{max} values for large commercial designs. As blade lengths continue to increase, transportation considerations will favor decreased values of c_{max}. However, the trends illustrated in Table 11 indicate that decreases in c_{max} must be traded against loss of structural efficiency and an associated increase in blade mass.
4. As the baseline blade configurations are scaled up, design modifications to reduce mass are constrained by considerations of aerodynamic performance, edge-bending fatigue, and tip deflections.

5. Once a design is essentially fixed, blade length increases will result in a mass-scaling exponent that is slightly lower than cubic.

Taken together, these results and trends indicate that commercial blades at the upper end of the current size range are already pushing the limit of what can be achieved with conventional materials and design. For even larger blades, avoiding a near-cubic mass increase may require basic changes in:

- Materials, such as carbon or glass/carbon hybrids
- Manufacturing processes that can yield better mean properties and/or reduced property scatter through improvements in fiber alignment, compaction, and void reduction
- Load-mitigating rotor designs.

The following section presents cost calculations for the baseline blade design, scaled over the range of 750 kW to 5 MW. For the scaling results presented in this report, the basic material and manufacturing process remained unchanged. As such, a reduction in mass will correspond to a reduction of production blade costs in the same proportion. This would not hold true for mass savings realized through changes in materials, process, and rotor design. In evaluating each such change, the implications on both mass and cost must be considered.

4.4 Power Performance and Energy Production Calculations

As discussed in Section 3, energy production from a variable-speed, active power control turbine will depend on the entire C_P-TSR curve and other parameters such as maximum tip speed, rotor diameter, air density, hub-height wind speed distribution, drivetrain efficiency, and turbine availability. To account for these variables, spreadsheet-based power performance and energy production calculations were performed.

Power performance calculations were performed for the baseline rotor planform (TSR_{Design} = 7, c_{max} = 9% R), assuming sea-level air density, a maximum tip speed of 65 m/s, and a specific rating of 0.44 kW/m^2. An efficiency curve was constructed to account for drivetrain losses in converting rotor to system power. Figure 16 shows the calculated power performance and rotor speed curves for a 5-MW rotor. Between cut-in wind speed and 9 m/s, the rotor speed is varied linearly to track the optimal rotor C_P. At 9 m/s, the tip speed reaches the maximum value of 65 m/s. For wind speeds between 9 m/s and rated power, the rotor speed is held constant and the rotor C_P deviates from its optimum value. At 12.5 m/s, the rotor reaches its rated (system) power, and it is assumed that pitch control is used to maintain constant power above this wind speed.

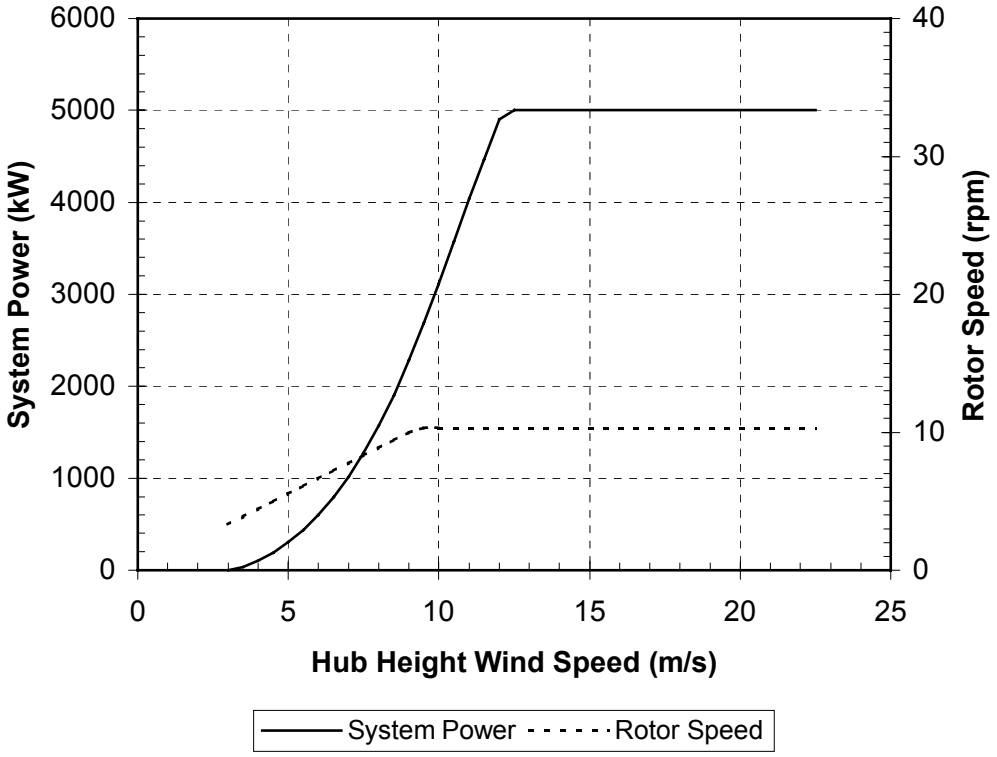

Figure 16. Power performance curve for 5-MW rotor

Annual energy production (AEP) calculations were performed by assuming Rayleigh wind speed distributions, with annual average wind speeds of 5.8 m/s at a height of 10 m. Hub height wind speed distributions were derived using a shear exponent of 1/7, and assuming that the turbine hub height scaled as 1.3 times the rotor diameter. The AEP calculations neglect array losses and assume 100% availability.

Figure 17 shows the calculated annual energy production, where the AEP values have been normalized to the swept area for each rotor. Over the range of sizes considered (750 kW to 5 MW), the mean hub height wind speed increases from 7.5 m/s to 8.6 m/s. Although the maximum theoretical energy available (per unit area) increases by 50% over this range, the calculated specific energy capture only increases by about 25% (primarily due to constrained peak power).

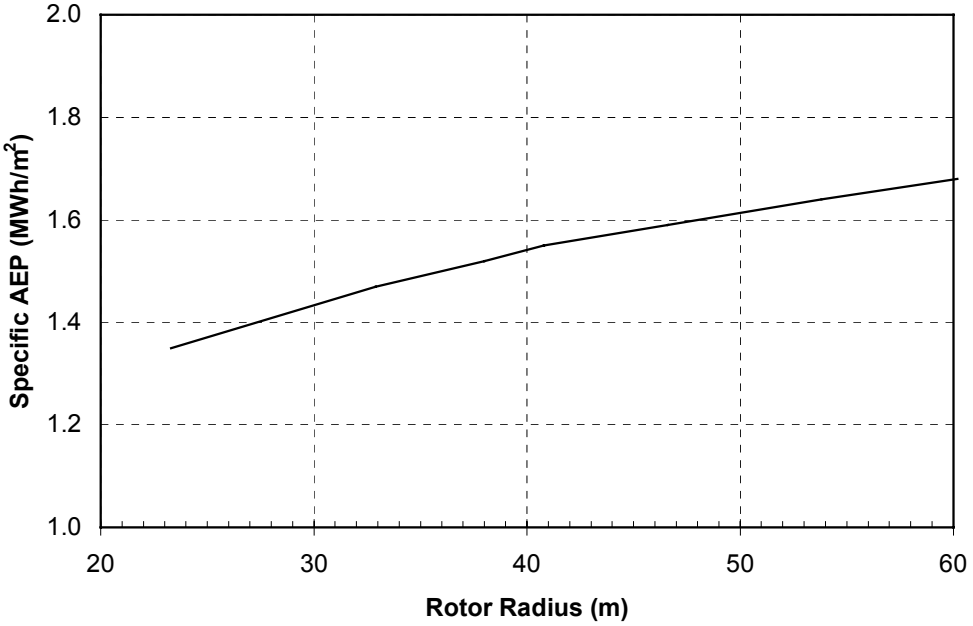

Figure 17. Calculated annual energy production for range of rotor sizes modeled

4.5 Cost Calculations

Cost calculations were performed using the equation set described in Section 2.9, with the structural scaling model output for rotors with $TSR_{Design} = 7$ and $c_{max} = 9\%$ R. As was discussed in that section, attaining a mature production rate requires a learning curve that is cycle-dominated. To illustrate the importance of this issue, cost estimates were made for rotors of 750 kW and 5 MW, using three different scenarios for the duration of the production runs.

The results of these estimates are summarized in Table 13. For all cases, a production rate of 200 MW/yr installed capacity was assumed. In the case of the 750-kW rotor, this equates to 800 blades per year, whereas, for the 5-MW rotor, 120 blades per year are produced. Table 13 indicates the average cost per blade, assuming production runs of varying duration. In all cases, fixed costs have been adjusted assuming a 10% interest rate over the period of production. Production rates are $10.45/kg, with the learning curve multipliers (as shown in Table 10) applied to the first 100 units. Simple averaging is then used to estimate the cost for each item over the assumed production run (total cost divided by total number of units).

Table 13. Cost Estimate for Varying Production-Run Scenarios

	750 kW Rotor			5 MW Rotor		
Cost Item	**1 Year**	**3 Year**	**5 Year**	**3 Year**	**5 Year**	**10 Year**
Total number of blades	800	2400	4000	360	600	1200
Average factor on prod. rate	1.11	1.04	1.02	1.24	1.14	1.07
Fixed cost per blade	$470	$170	$115	$10,730	$7,180	$4,370
Recurring cost per blade	$20,710	$19,370	$19,100	$343,050	$316,590	$296,750
Total cost per blade	$21,180	$19,540	$19,215	$353,780	$323,770	$301,140
Rotor (3 blades only) $/kW	$84.70	$78.20	$76.90	$212.30	$194.30	$180.70

As seen in Table 13, the impact of the learning curve on the 750-kW blade costs is fairly subtle. For a one-year production run, the cost increase due to this effect is about 11%, and if averaged over three years of production, would drop to 4%. However, as a result of the lower number of production cycles, the learning curve effect has a much greater impact on the costs for the 5-MW rotor. For an assumed production run of three years, the cost increase for 5-MW blades is 24%, and drops to 14% and 7%, respectively, for production runs of 5 and 10 years.

The fixed costs are generally a minor fraction of the total blade costs, and, as expected, this fraction decreases with increased number of items produced. There is also a moderate escalation in fixed costs as the rotors grow larger. For the five-year production scenario, the fixed-costs fractions are 0.6% and 2.2% of the total blade costs, respectively, for the 750-kW and 5-MW rotors.

A five-year production scenario was selected for estimating blade costs over the full range of ratings between 750 kW and 5 MW. The results are summarized in Table 14. The rotor radius and rating are input to both the structural design and cost models. The blade surface area is calculated for the blade geometry being modeled (TSR_{Design} = 7, c_{max} = 9% R). The mass values are output from the structural design model, and in turn, serve as input to the cost model. The AEP values indicated by Figure 17 were used to calculate the cost per MWh. In all of the following tables, figures, and discussion, the term "rotor costs" refers to a set of three blades, including the root connection but excluding costs for the other hub hardware.

Table 14. Blade Mass and Cost for Rotors between 750 kW and 5 MW (5-year production)

Radius	Rating	Area*	Mass (kg)		Average Cost per Blade			Rotor Costs	
(m)	(kW)	(m^2)	Blade	Root	Fixed	Prod.	Total	$/kW	$/MWh/yr
23.3	750	66.3	1577	111	$115	$19,100	$19,215	$76.9	$25.1
32.9	1500	132.6	4292	243	$520	$51,850	$52,370	$104.7	$31.4
38.0	2000	176.8	6528	336	$970	$79,230	$80,200	$120.3	$34.9
40.8	2300	203.3	8010	388	$1,320	$97,495	$98,815	$128.9	$36.6
46.6	3000	265.2	11,783	515	$2,350	$144,910	$147,260	$147.3	$40.8
53.8	4000	353.6	17,961	681	$4,405	$224,395	$228,800	$171.6	$46.0
60.2	5000	442.0	24,869	851	$7,180	$316,590	$323,770	$194.3	$50.8

* Blade surface area

To assist with the interpretation of Table 14, scaling exponents were developed for several key cost and performance parameters. The exponents were developed for the range between approximately 2.3 and 5.0 MW (radius ranging from 40.8 to 60.2 m). The results are presented in Table 15; the scaling function for each parameter is given by Equation 9.

$$\frac{Parameter}{Parameter_o} = \left(\frac{R}{R_o} \right)^{Exp} \qquad \text{(Eqn. 9)}$$

where

$Parameter/Parameter_o$ ≡ ratio of each parameter to its value at R = 40.8 m
R/R_o ≡ ratio of rotor radius to R = 40.8 m
EXP ≡ scaling exponent.

Table 15. Scaling Exponents for Range of 2.3 to 5.0 MW

Parameter	Scaling Exponent
Energy production	2.22
Blade mass	2.87
Blade costs	3.03
Rotor cost per kW capacity ($/kW)	1.04
Rotor cost per energy capture ($/MWh/yr)	0.82

Due to the assumed increase in hub height with rotor size and associated wind shear, the energy capture scales more rapidly than the rotor swept area (exponent of 2.22). Because the scaling was performed for a fixed-blade design, the mass exponent is slightly less than cubic. However, due to the impact of the learning-curve costs on the five-year production scenario, the blade cost exponent is slightly greater than cubic. The blade cost per installed kilowatt is shown to increase in a near-linear fashion with radius, and the cost per energy capture scales as the radius to an exponent of 0.82.

The cost estimates presented above are appropriate for the assumptions and design modeled. Indeed, the same general trend would result for any fixed-blade design that is scaled over the same range of ratings. To realize lower exponents on blade cost and mass would require evolution of the design and/or manufacturing process as the rotors become larger.

5. Conclusions

In this report, the scaling of current materials and manufacturing technologies for blades of 40 to 60 meters in length was investigated. Direct design calculations were used as a basis for constructing a computational blade-scaling model. The model was then used to calculate structural properties for a wide range of aerodynamic designs and rotor sizes. Industry manufacturing experience was used to develop cost estimates, based on blade mass, surface area, and the duration of the assumed production run.

The structural design model was used to perform a series of parametric analyses. The results quantify the mass and cost savings possible for specific modifications to the baseline blade design, demonstrate the aerodynamic and structural trade-offs involved, and identify the constraints and practical limits to each modification.

Scaling results were compared with mass data for current commercial blades. For a given blade design, the modeled blade mass and costs scale as a near-cubic of rotor diameter. In contrast, commercial blade designs have maintained a scaling exponent closer to 2.4 for lengths ranging between 20 and 40 meters. Results from the scaling study indicate that:

- To realize this lower scaling exponent on cost and mass has required significant evolution of the aerodynamic and structural designs.
- Commercial blades at the upper end of the current size range are already pushing the limits of what can be achieved using conventional manufacturing methods and materials.
- For even larger blades, avoiding a near-cubic mass increase may require fundamental changes in:
  - Materials, such as carbon or glass/carbon hybrids.
  - Manufacturing processes that can yield better mean properties and/or reduced property scatter through improvements in fiber alignment, compaction, and void reduction. The extent to which improved material properties can reduce blade mass and cost may be limited by stiffness requirements for the blade structure.
  - Load-mitigating rotor designs.

For the scaling results presented in this report, the basic material and manufacturing process remained unchanged. As such, a reduction in mass will correspond to a reduction of production blade costs in the same proportion. However, this will not hold true for mass savings realized through changes in materials, process, and rotor design. In evaluating each such change, the implications on both mass and cost must be considered.

The learning curve required to achieve a mature production process has a meaningful effect on blade costs for the range of rotor sizes considered. A production rate of 200 MW per year implies 800 blades at 750 kW, but only 120 blades at 5 MW. Therefore, the cost penalty for initial production cycles has an increasing impact on the first-year production costs as rotor sizes increase; a complete cost assessment depends on both annual production rates and the extent (number of years) of sustained production.

6. References

1. Global Energy Concepts, LLC. (November, 2000). GEC database of blade specifications for megawatt scale turbines, from a combination of published and non-published sources.
2. International Electrotechnical Commission. (1999). *IEC 61400-1: Wind turbine generator systems—Part 1: Safety Requirements*, 2nd Edition. International Standard 1400-1.
3. Harrison, R.; Jenkins, G. (1994). *Cost Modeling of Horizontal axis Wind Turbines*, for ETSU W/34/00170/REP. University of Sunderland, UK.
4. Giguere, P.; Selig, M.S. (January 10-13, 2000). *Blade Geometry Optimization for the Design of Wind Turbine Rotors*. Proceedings of AIAA/ASME Wind Energy Symposium. Reno, NV.
5. Tangler, J.L.; Somers, D.M. (March 26-30, 1995). "NREL Airfoil Families for HAWTs". Presented at the American Wind Energy Association Windpower '95 Conference. Washington, DC.
6. Eppler, R.; Somers, D.M. (1980). *A Computer Program for the Design and Analysis of Low-Speed Airfoils*. NASA TM-80210. National Aeronautics and Space Administration.
7. Selig, M.S.; Tangler, J.L. (May 10-13, 1994). "A Multipoint Inverse Design Method for Horizontal Axis Wind Turbines", Presented at the AWEA Windpower '94 Conference. Minneapolis, MN.
8. Sommer, J. (May 12, 2000). Laminate test data from faxed correspondence to GEC.
9. Mandell, J.F.; Samborsky, D.D. (1997). "*DOE/MSU Composite Material Fatigue Database: Test Methods, Materials and Analysis*." SAND97-3002.
10. Germanischer Lloyd. (1999). Rules and Regulations IV—Non-Marine Technology, Part 1—Wind Energy, *Regulation for the Certification of Wind Energy Conversion Systems*.
11. Malcolm, D. (June 2000). Calculations based on curves supplied by J. Mandell, from Excel spreadsheet "SNcurvesDM.xls".
12. Sommer, J. (August 14, 2000). Private written correspondence with GEC.
13. Griffin, D.A. (August 2000). *NREL Advanced Research Turbine (ART) Aerodynamic Design of ART-2B Rotor Blades*. NREL/SR-500-28473. Golden, CO: National Renewable Energy Laboratory.

REPORT DOCUMENTATION PAGE

Form Approved
OMB NO. 0704-0188

1. AGENCY USE ONLY (Leave blank)	2. REPORT DATE	3. REPORT TYPE AND DATES COVERED
	April 2001	Subcontract Report

4. TITLE AND SUBTITLE
WindPACT Turbine Design Scaling Studies Technical Area 1—Composite Blades for 80- to 120-Meter Rotor

5. FUNDING NUMBERS
YAM-0-30203-01

6. AUTHOR(S)
Dayton A. Griffin

7. PERFORMING ORGANIZATION NAME(S) AND ADDRESS(ES)
Global Energy Concepts, LLC
5729 Lakeview Drive NE, #100
Kirkland, WA 98033

8. PERFORMING ORGANIZATION REPORT NUMBER

9. SPONSORING/MONITORING AGENCY NAME(S) AND ADDRESS(ES)
National Renewable Energy Laboratory
1617 Cole Blvd.
Golden, CO 80401-3393

10. SPONSORING/MONITORING AGENCY REPORT NUMBER
NREL/SR-500-29492

11. SUPPLEMENTARY NOTES
NREL Technical Monitor: Alan Laxson

12a. DISTRIBUTION/AVAILABILITY STATEMENT
National Technical Information Service
U.S. Department of Commerce
5285 Port Royal Road
Springfield, VA 22161

12b. DISTRIBUTION CODE

13. ABSTRACT *(Maximum 200 words)* The United States Department of Energy (DOE) through the National Renewable Energy Laboratory (NREL) implemented the Wind Partnership for Advanced Component Technologies (WindPACT) program. As part of the WindPACT program, Global Energy Concepts, LLC (GEC), was awarded contract number YAM-0-30203-01 to examine Technical Area 1—Blade Scaling, Technical Area 2—Turbine Rotor and Blade Logistics, and Technical Area 3—Self-Erecting Towers. This report documents the results of GEC's Technical Area 1—Blade Scaling. The primary objectives of the Blade-Scaling Study are to assess the scaling of current materials and manufacturing technologies for blades of 40 to 60 meters in length, and to develop scaling curves of estimated cost and mass for rotor blades in that size range.

14. SUBJECT TERMS
wind energy; WindPACT; turbine rotor; blades

15. NUMBER OF PAGES

16. PRICE CODE

17. SECURITY CLASSIFICATION OF REPORT	18. SECURITY CLASSIFICATION OF THIS PAGE	19. SECURITY CLASSIFICATION OF ABSTRACT	20. LIMITATION OF ABSTRACT
Unclassified	Unclassified	Unclassified	UL